

Supplementary Information

Non-equilibrium Insertion of Lithium Ions into Graphite

Na Li,^{†a,b} Ming-Zi Sun,^{†c} Sooyeon Hwang,^b Shuang Li,^b Hong-Yang Zhao,^a Ya-Ping Du,^{*d} Bo-Long Huang^{*c} and Dong Su^{*e}

^a Key Laboratory of Shaanxi for Advanced Materials and Mesoscopic Physics, School of Physics, Xi'an Jiaotong University, No. 28 West Xianning Road, Xi'an 710049, China.

^b Center for Functional Nanomaterials, Brookhaven National Laboratory, Upton, New York 11973, United States.

^c Department of Applied Biology and Chemical Technology, The Hong Kong Polytechnic University, Hong Hum, Kowloon, Hong Kong SAR, China.
E-mail: bhuang@polyu.edu.hk

^d School of Materials Science and Engineering & National Institute for Advanced Materials, Nankai University, Tianjin 300350, China.
E-mail: ypdu@nankai.edu.cn

^e Beijing National Laboratory for Condensed Matter Physics, Institute of Physics, Chinese Academy of Sciences, Beijing, 100190, China.
E-mail: dongsu@iphy.ac.cn

[†] These authors contributed equally to this work

Experimental Section/Methods

Materials: Graphite (nanoparticle, natural, thickness: 40 nm, lateral size: 400-600 nm) was purchased from ACS Material Store and used without any further purification. The solvents of ethanol, dimethyl carbonate (DMC) and N-methyl-2-pyrrolidone (NMP) were in ACS reagent grade and were purchased from Fisher Scientific and used without further purification.

TEM Characterization: The in-situ TEM electrochemical dry cell was incorporated into a Nanofactory TEM-STM specimen holder (shown in Fig. 2a), in which graphite dispersed onto a TEM half-grid with amorphous carbon support are analogous to the active electrode. The lithium metal is coated onto a piezo-driven tungsten (W) probe, which acts as the counter electrode. The graphite and Li were loaded onto the holder in an Ar-filled glove box, and the sample holder is transferred from an Ar-filled sealed container to the microscope within several seconds. During those seconds, a thin layer of Li_2O is formed on Li metal, which could be used as the solid electrolyte in the dry cell. During the in-situ lithiation, a constant negative DC potential (1.5 V) was applied to the specimen, and the lithiation processes were captured by real-time imaging in SAED mode with a JEM-2100F transmission electron microscope (JEOL) at an acceleration voltage of 200 kV. Electron-energy loss spectroscopy (EELS) was conducted on JEM-2100F operated at 200 kV. In order to make the electron beam below the threshold of damage the C atoms in graphite, the in-situ HRTEM image was obtained in a Titan 80-300 transmission electron microscope (FEI) at an acceleration voltage of 80 kV,¹ which has an objective-lens aberration corrector and a spatial resolution of 1.5 Å in the high-resolution phase-contrast mode. The ex-situ samples after discharge in coin cells were examined accordingly.

Electrochemical Measurement: The electrodes were prepared with 90 wt % active material (graphite), 5 wt % acetylene carbon black, and 5 wt % polyvinylidene fluoride (PVDF) in N-methyl-2-pyrrolidone (NMP) and cast onto copper foil current collectors using a doctor blade. The electrodes were dried in the dry room at room temperature for 24 hours. The 2032-type coin cells were assembled in an argon-filled glove box using the composite electrode as the positive electrode and Li metal as the negative, electrode with Celgard (2325) separator in between to prevent shorting. The electrolyte was lithium hexafluorophosphate (LiPF_6) (1M) in ethylene carbonate/dimethyl carbonate (EC/DMC) (volume ratio 50:50). The electrochemical measurements were conducted at room temperature using a Biologic (VMP3) battery cycler. The cells were cycled galvanostatically at 0.1 C and 10 C between 0.01 and 3.0 V, respectively.

XRD/Raman Characterization: The X-ray diffraction (XRD) patterns were collected on Ultima III XRD/XRR diffractometer (Cu K α radiation, $\lambda = 1.54056 \text{ \AA}$) at room temperature. The samples after discharge (0.1 C-rate/10 C-rate after 10 cycles) were sealed in 0.5 mm thickness scotch tape inside the glovebox, and diffraction patterns were measured in a 2θ range = $15\text{-}45^\circ$ with a step size of 0.01° and step speed of $1^\circ/\text{min}$. The zinc powders (6-8 micron, P6₃/mmc space group) were used as the reference peaks to demonstrate that the graphite peak shifting was electrochemical in nature not an artifact of mechanical tests. Additional analysis was performed by Raman spectroscopy (WiT37ec Probe Microscope) using 532 nm laser radiation.

Calculation Setup: In this molecule dynamic simulation, CASTEP codes² with Broyden-Fletcher-Goldfarb-Shannon (BFGS) algorithm was selected for geometry optimization during the dynamic simulations. The cut-off energy for PBE³ with GGA^{4,5} functions is set to be 750 eV with a plane-wave basis set. The model of graphite inserted with lithium atom is a $7\times 7\times 2$ supercell of graphite with 392 carbon atoms. To discover the dynamic simulation with different situations, we have applied disorder lithium atom models in the graphite model with 78 lithium atoms randomly distributed among four layers of graphite. For dynamic simulation, we choose NVT (*i.e. a dynamic study at fixed volume with a thermostat to maintain a constant temperature*) mode under 300K with constant volume. Each step has been set as 1 fs in the disorder models. For the NPT (*i.e. a dynamic study with a thermostat to maintain a constant temperature and with a barostat to maintain a constant pressure*) mode, the dynamic simulation environment has been set at 300K with constant pressure. NPT model has applied the electric field of 1.5 V/m on [010] direction to observe the influence of the external electric field. NVT model has been operated under non-electrical field condition and same electrical field condition as NPT.

For all the defect formation, a $4\times 4\times 1$ graphite unit cell has been constructed to build the defect in the cell for geometry optimization. For geometry optimization of the defective structure and distorted graphite unit cell, a 380 eV with ultrasoft pseudopotential setting has been chosen. Within this setting, the maximum energy on every atom is 5×10^{-5} eV with max force 0.1 eV/\AA .

Supporting Movies Showing the Structural Evolution of the Graphite upon Li Insertion

Video S1: In-situ electron diffraction pattern during the entire lithiation process. The movie is accelerated by 290 times (AVI).

Video S2: In-situ HRTEM showing the non-equilibrium lithiation process via intercalation reactions. The movie is accelerated by 20 times (AVI).

Supplementary Figures

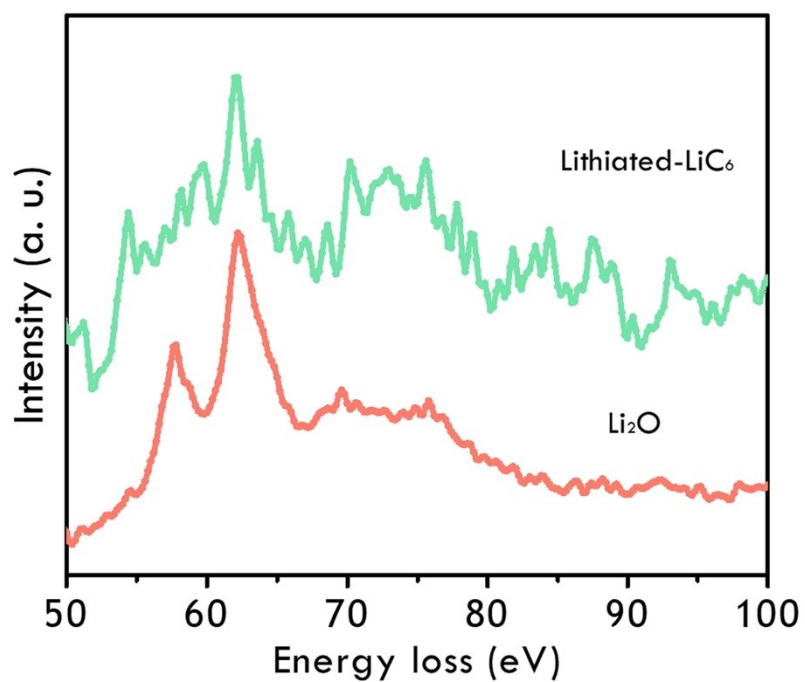


Fig. S1. Evolution of graphite EELS during in-situ lithiation. EELS spectra showing low-loss characteristic energy edges Li-K profiles obtained at Li₂O and fully-lithiated graphite regions, similar to the literature.⁶

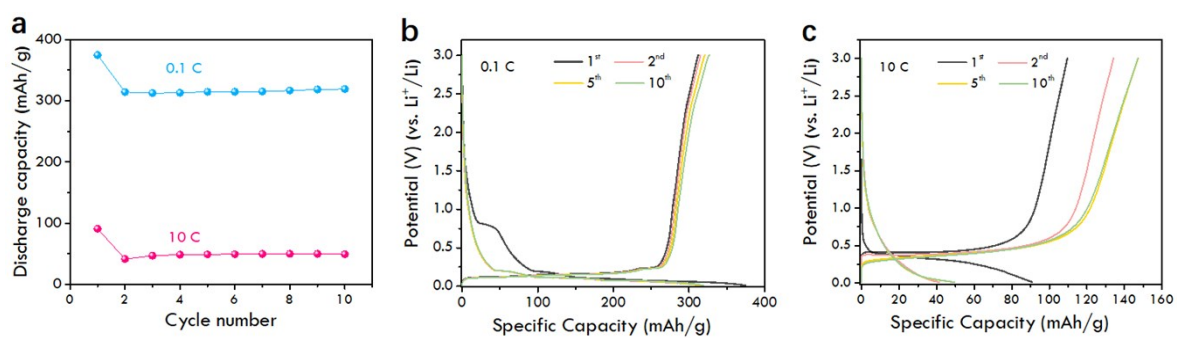


Fig. S2. Electrochemical performance of the graphite half-cell test. (a) Cyclic properties at 0.1 C and 10 C. Charge/discharge curves at (b) 0.1 C and (c) 10 C.

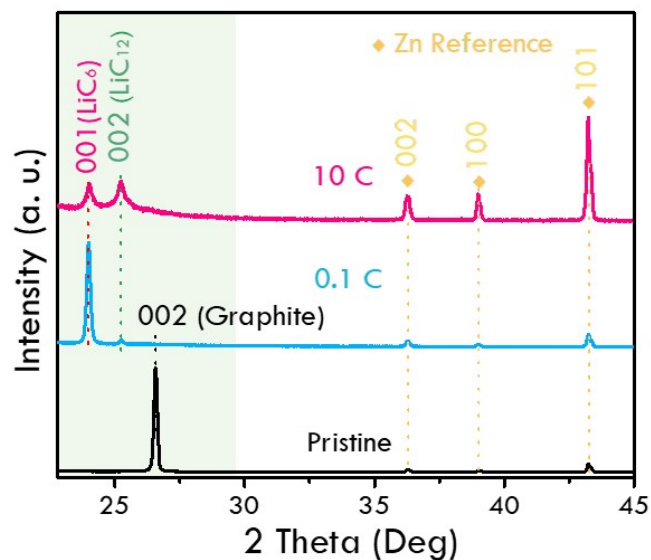


Fig. S3. XRD spectra of pristine, 0.1 C-rate and 10 C-rate graphite. The peaks at 2-theta of 36.29°, 38.99° and 43.23° correspond to (002), (100), (101) direction of the zinc powders (6-8 micron, P63/mmc space group), which were used as the reference peaks to demonstrate that the graphite peak shifting was electrochemical in nature not an artifact of mechanical tests. With the intercalation of Li-ion, as shown of the inset photographs, the color of graphite electrode became gold yellow, which indicates the formation of LiC₆.⁷

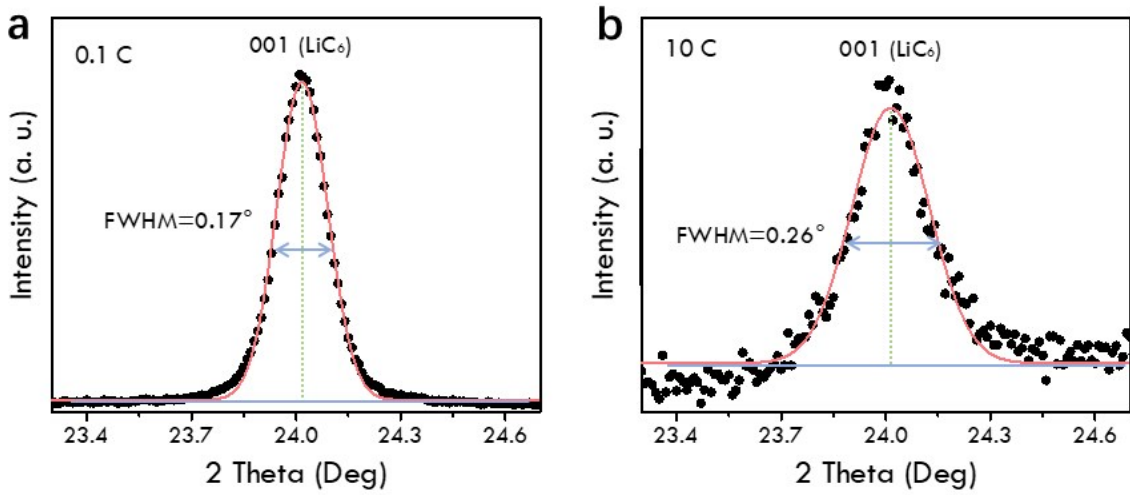


Fig. S4. Intensity profiles of ex-situ XRD spectra. (a) 0.1 C-rate and (b) 10 C-rate graphite with Gaussian fitting. The Scherrer equation (1) was used to determine the crystallite size of graphite at different current rate.⁸

$$D = \frac{k\lambda}{\beta \cos \theta} \quad (1)$$

Where D is the crystallite size, k is a numerical factor ($k=0.89$), λ is the X-ray wavelength ($\lambda_{Cu\ ka} = 0.154056$ nm), β is the full width at half maximum (FWHM) of the X-ray diffraction peak in radians and θ is the Bragg angle. The D of 0.1 C-rate is ~ 51 nm and 10 C-rate is ~ 33 nm.

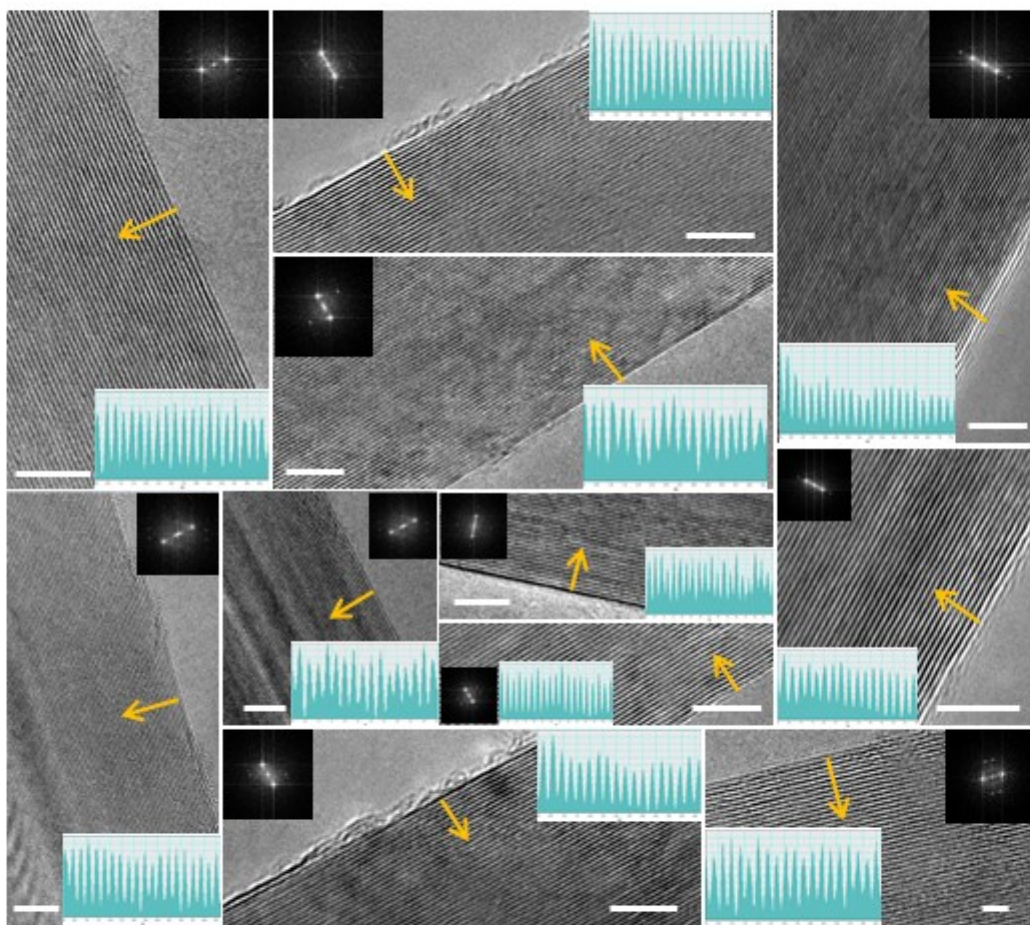


Fig. S5. HRTEM images obtained from the pristine graphite electrode. Scale bars, 5 nm. Each of the representative images was carried out in a stochastic pattern without any cherry-picking, which ensures the statistical nature of the true reaction modalities. Corresponding FFT pattern and line profile along the arrow are shown at each image.

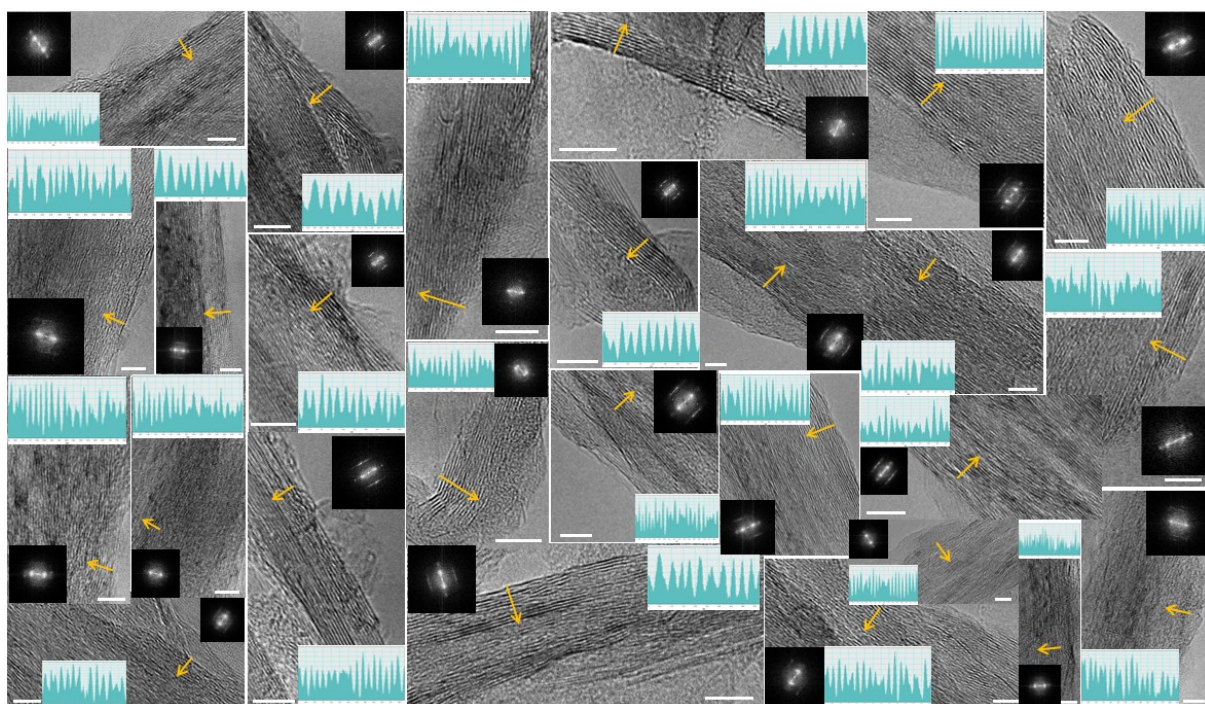


Fig. S6. HRTEM images obtained from the discharged sample at 0.1 C-rate after 10 cycles. Scale bars, 5 nm. Corresponding FFT pattern and line profile along the arrow are shown at each image.

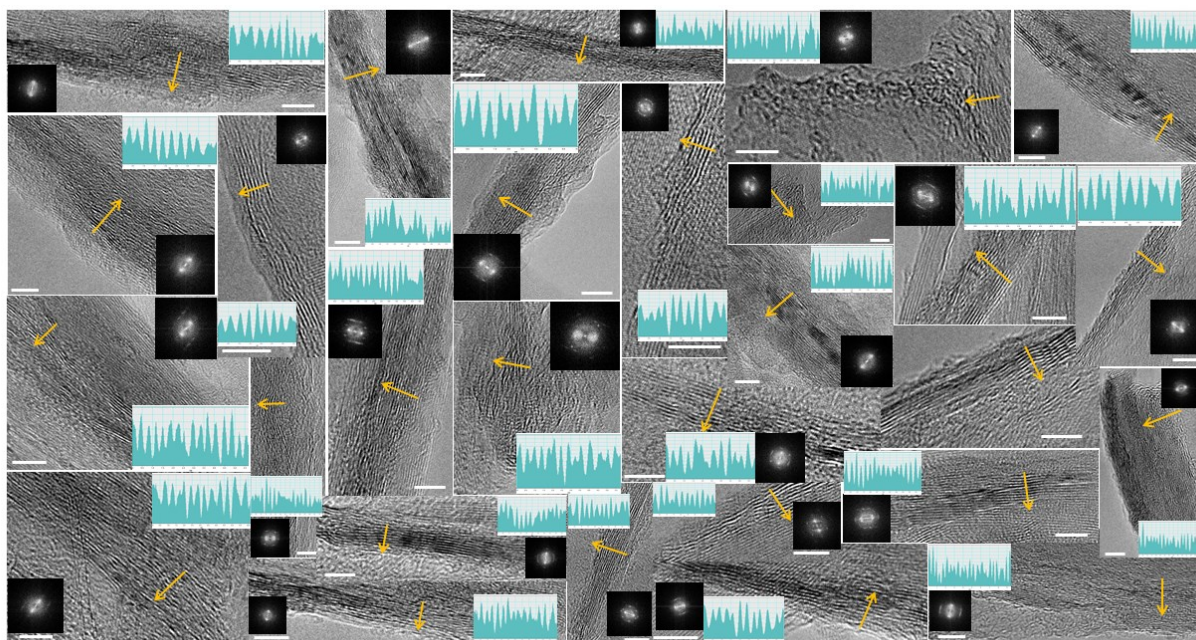


Fig. S7. HRTEM images obtained from the discharged sample at 10 C-rate after 10 cycles. Scale bars, 5 nm. Corresponding FFT pattern and line profile along the arrow are shown at each image.

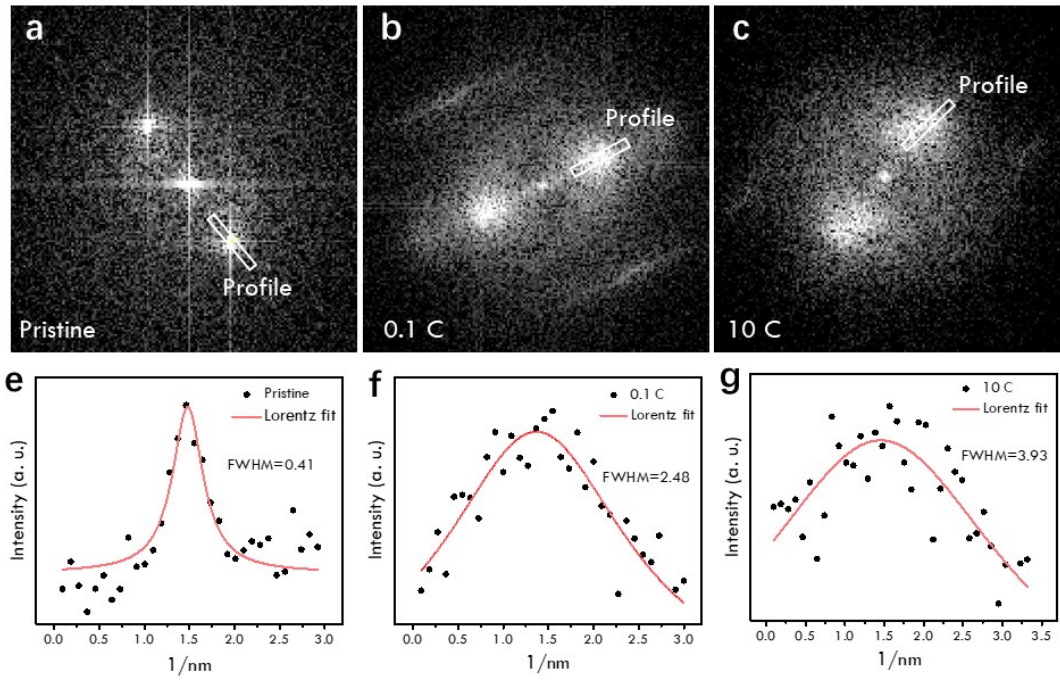


Fig. S8. (a), (b) and (c) The FFT results from Fig. 3d-f. (d), (e) and (f) Intensity profiles of Bragg reflection from FFT with Lorentz fitting.

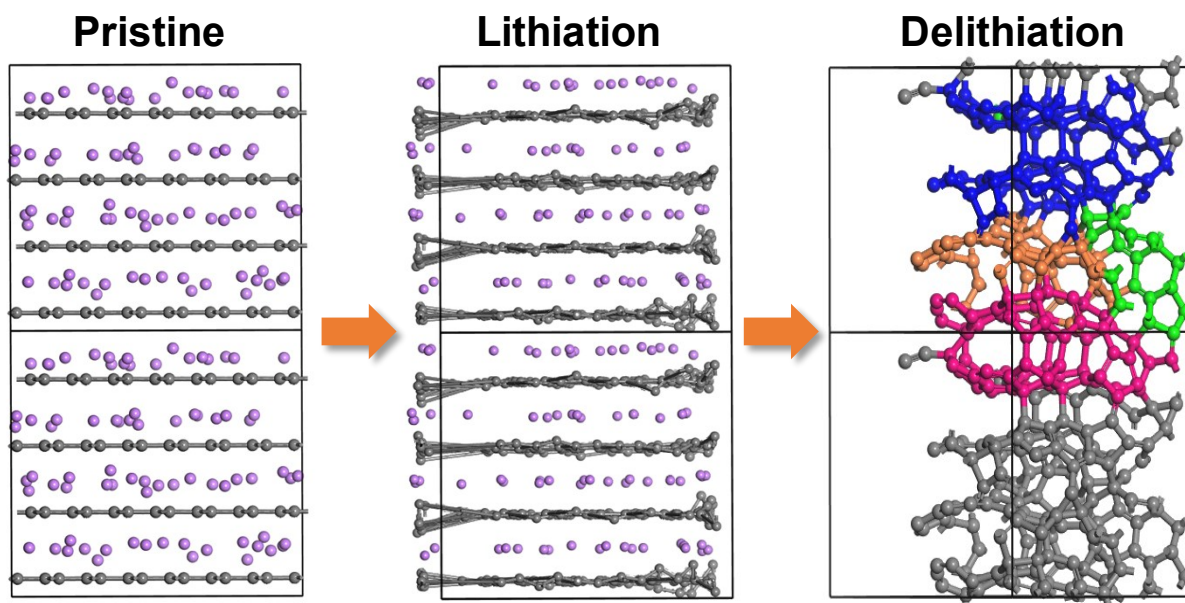


Fig. S9. The lithiation and delithiation process of graphite under 1.5 V electrical field on [010] direction. Pristine: the pristine structure of graphite with randomly distributed lithium ions. Lithiation: the dynamic simulation of the pristine structure under 1.5 V electrical field after 225 fs. Delithiation: the fully relaxed structure of graphite after removing lithium ions as the discharge process. The color marked lattice structure in the final delithiation step represents the “Fullerenalization” of graphite with semi-cage structure in theoretical simulations, which forms after the full relaxation of graphite by removing all the lithium ions.

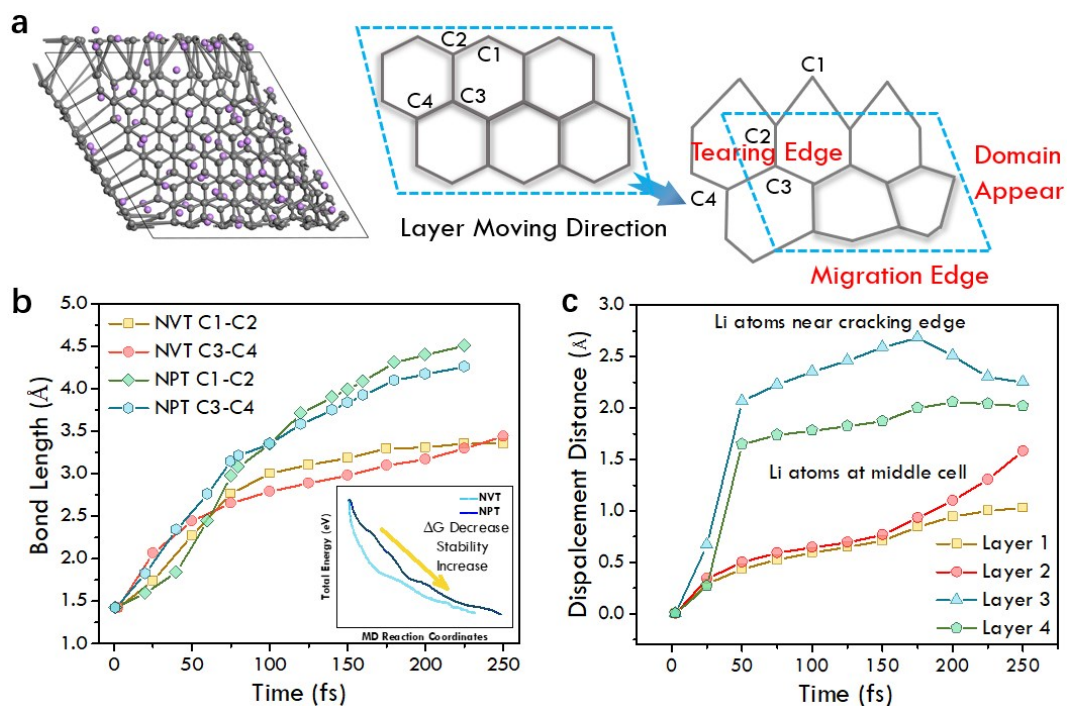


Fig. S10. (a) Illustration of the formation of tearing domains. (b) Bond length change near the cracking edge. (c) Diffusion distance of lithium atoms at different positions of the graphite unit cell in disorder model under NVT.

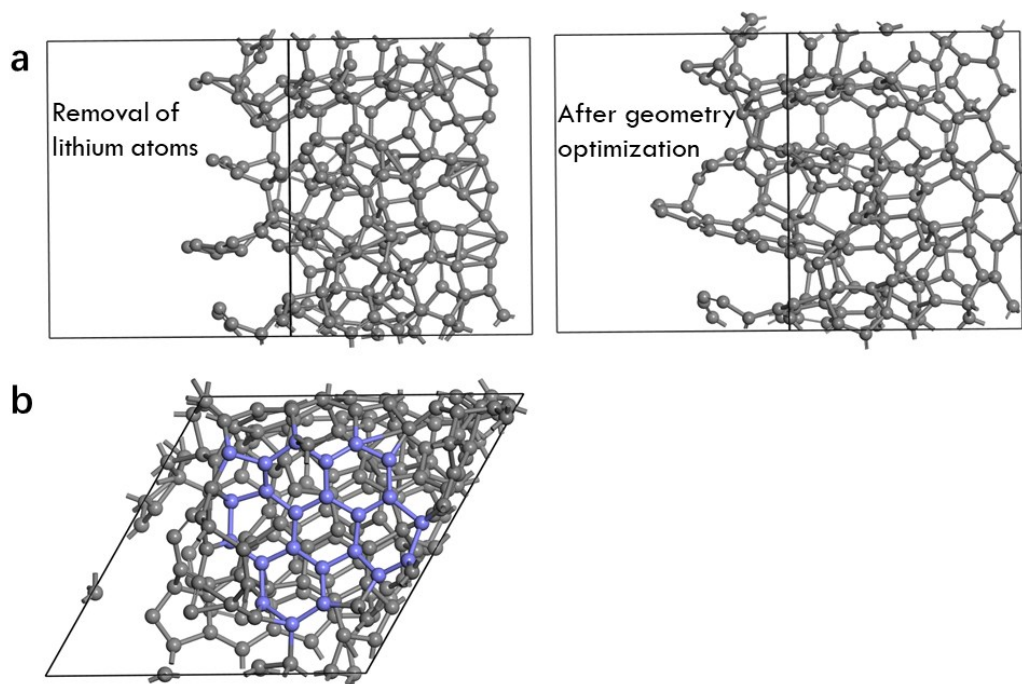


Fig. S11. Relaxed structure of distorted graphite layer after removal of Li ions. (a) Comparison of structures before and after geometry relaxation. (b) The partial preservation of local graphite structure after relaxation.

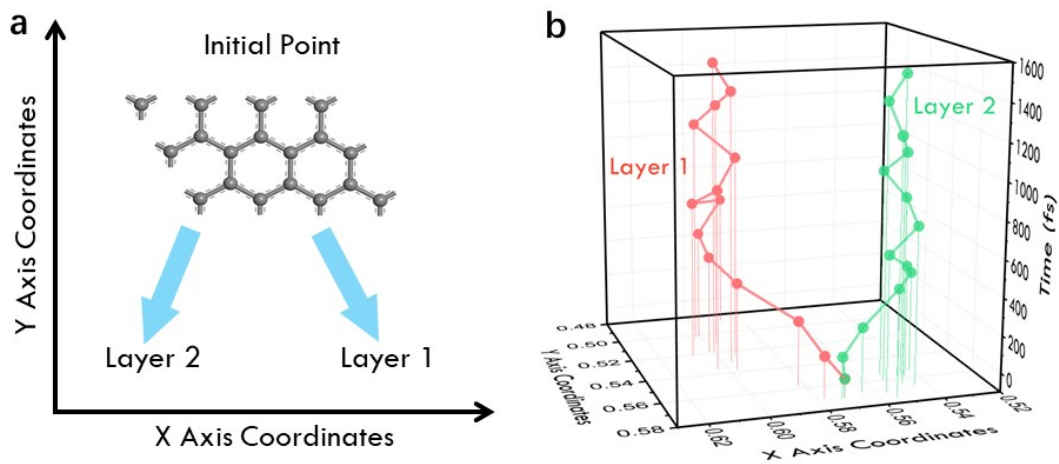


Fig. S12. The dynamic layer movements of graphite with randomly distributed Li ions with no electrical field. (a) Moving direction of neighboring layers. (b) Moving trajectory of selected carbon atoms on neighboring layers.

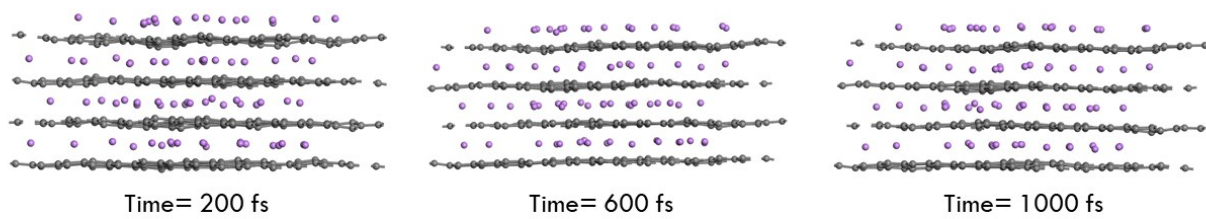


Fig. S13. The side view of the dynamic configuration of disorder lithium atoms model at different simulation time without electrical field.

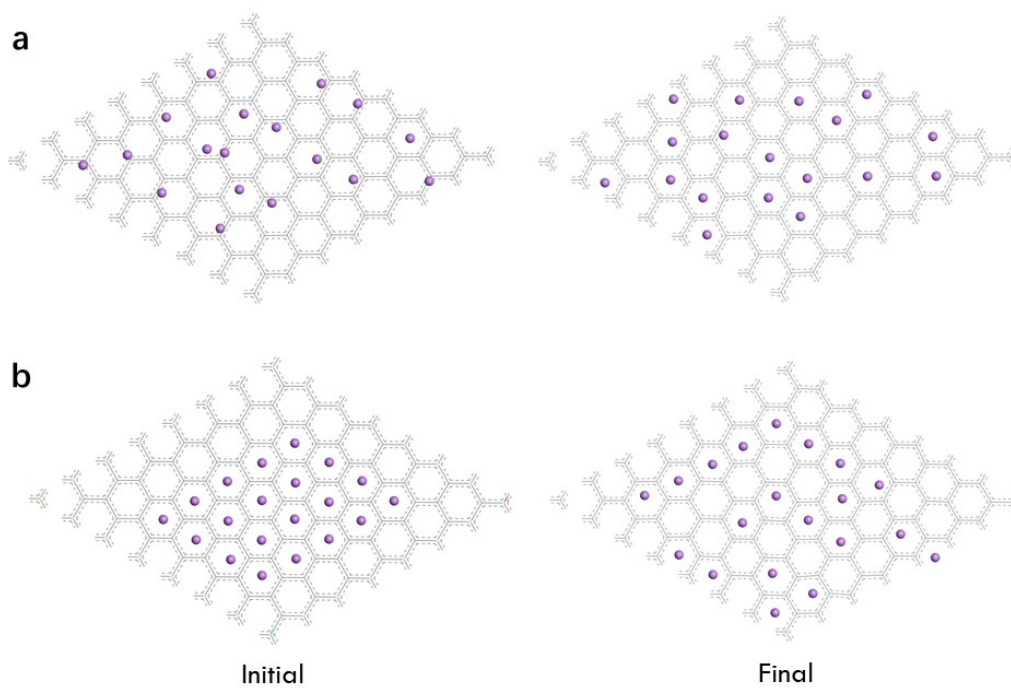


Fig. S14. Migrations of Li atoms on Layer 1 of graphite. (a) Disorder model. (b) Ordered model.

References

- 1 J. C. Meyer, F. Eder, S. Kurasch, V. Skakalova, J. Kotakoski, H. J. Park, S. Roth, A. Chuvilin, S. Eyhusen, G. Benner, A. V. Krasheninnikov, U. Kaiser, *Phys. Rev. Lett.* 2012, **108**, 196102.
- 2 S. J. Clark, D. S. Matthew, J. P. Chris, J. H. Phil, I. J. P. Matt, R. Keith, C. P. Mike, *Zeitschrift Fur Kristallographie* 2005, **220**, 567-570.
- 3 J. D. Head, M. C. A. Zerner, *Chem. Phys. Lett.* 1985, **122**, 264-270.
- 4 J. P. Perdew, K. Burke, M. Ernzerhof, *Phys. Rev. Lett.* 1996, **77**, 3865-3868.
- 5 J. P. Perdew, J. A. Chevary, S. H. Vosko, K. A. Jackson, M. R. Pederson, D. J. Singh, C. *Phys. Rev. B* 1992, **46**, 6671-6687.
- 6 A. Hightower, C. C. Ahn, B. Fultz, P. Rez, *Appl. Phys. Lett.* 2000, **77**, 238-240.
- 7 S. J. Harris, T. Timmons, D. R. Baker, C. Monroe, *Chem. Phys. Lett.* 2010, **485**, 265-274.
- 8 P. Scherrer, *Göttinger Nachrichten Math. Phys.* 1918, **2**, 96-100.